Wafer-scale 4H-silicon carbide-on-insulator (4H–SiCOI) platform for nonlinear integrated optical devices

Yi, Ailun; Zheng, Yi; Huang, Hao; Lin, Jiajie; Yan, Youquan; You, Tiangui; Huang, Kai; Zhang, Shibin; Shen, Chen; Zhou, Min

Total number of authors:
15

Published in:
Optical Materials

Link to article, DOI:
10.1016/j.optmat.2020.109990

Publication date:
2020

Document Version
Peer reviewed version

Journal Pre-proof

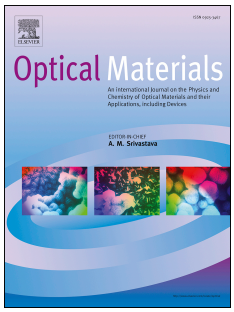

Wafer-scale 4H-silicon carbide-on-insulator (4H–SiCOI) platform for nonlinear integrated optical devices

Ailun Yi, Yi Zheng, Hao Huang, Jiajie Lin, Youquan Yan, Tiangui You, Kai Huang, Shibin Zhang, Chen Shen, Min Zhou, Wei Huang, Jiaxiang Zhang, Shengqiang Zhou, Haiyan Ou, Xin Ou

PII: S0925-3467(20)30335-9

DOI: https://doi.org/10.1016/j.optmat.2020.109990

Reference: OPTMAT 109990

To appear in: *Optical Materials*

Received Date: 9 February 2020

Revised Date: 2 April 2020

Accepted Date: 4 May 2020

Please cite this article as: A. Yi, Y. Zheng, H. Huang, J. Lin, Y. Yan, T. You, K. Huang, S. Zhang, C. Shen, M. Zhou, W. Huang, J. Zhang, S. Zhou, H. Ou, X. Ou, Wafer-scale 4H-silicon carbide-on-insulator (4H–SiCOI) platform for nonlinear integrated optical devices, *Optical Materials* (2020), doi: https://doi.org/10.1016/j.optmat.2020.109990.

Credit Author Statement

Ailun Yi Conceptualization, Validation, Resources, Validation, Investigation, Formal analysis, Writing - Original Draft, Visualization, Writing - Review & Editing

Yi Zheng Methodology, Investigation, Formal analysis, Data Curation, Formal analysis, Writing - Review & Editing

Hao Huang Investigation

Jiajie Lin Writing - Review & Editing

Youquan Yan Methodology, Validation

Tiangui You Project administration,

Kai Huang Methodology, Supervision

Shibin Zhang Formal analysis

Chen Shen Resources

Min Zhou Resources, Investigation

Wei Huang Supervision

Jiaxiang Zhang Supervision, Writing - Review & Editing

Shengqiang Zhou Supervision, Writing - Review & Editing

Haiyan Ou Supervision, Writing - Review & Editing, Funding acquisition

Xin Ou* Supervision, Project administration, Writing - Review & Editing, Funding acquisition

Graphical Abstract

We demonstrated 4-inch wafer-scale single-crystalline 4H-SiC film integrated with Si (100) substrate serves as a platform for nonlinear integrated optical devices. Micro-ring resonator devices with Q value of 6.6×10^4 based on 4H-SiCOI platform were further fabricated.

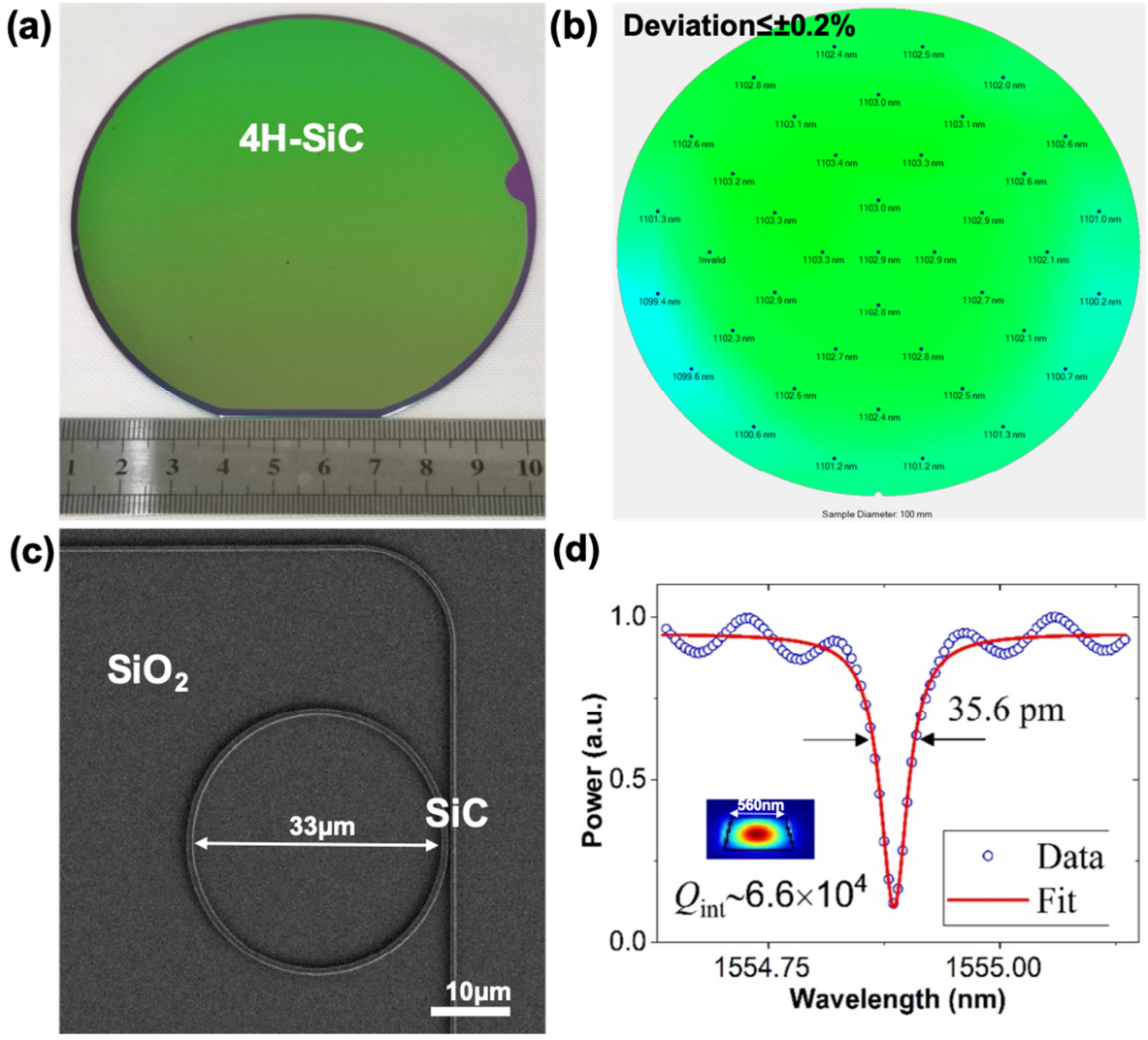

Wafer-scale 4H-silicon carbide-on-insulator (4H-SiCOI) platform for nonlinear integrated optical devices

*Ailun Yi[1,4], Yi Zheng[2], Hao Huang[1,4], Jiajie Lin[1,4], Youquan Yan[1,4], Tiangui You[1], Kai Huang[1], Shibin Zhang[1,4], Chen Shen[1], Min Zhou[1], Wei Huang[5], Jiaxiang Zhang[1], Shengqiang Zhou[3], Haiyan Ou[2], Xin Ou[1,4]**

[1]State Key Laboratory of Functional Materials for Informatics,
Shanghai Institute of Microsystem and Information Technology,
Chinese Academy of Sciences, Shanghai, 200050, People's Republic of China
[2]DTU Fotonik, Technical University of Denmark, Building 343, DK-2800 Lyngby, Denmark
[3] Institute of Ion Beam Physics and Materials Research, Helmholtz-Zentrum Dresden-Rossendorf, Bautzner Landstrasse 400, Dresden 01328, Germany.
[4]Center of Materials Science and Optoelectronics Engineering,
University of Chinese Academy of Sciences, Beijing, 100049, People's Republic of China
[5]Shanghai Institute of Ceramics,
Chinese Academy of Sciences, Shanghai 201800, People's Republic of China
*Corresponding author email: ouxin@mail.sim.ac.cn

Abstract

4H-silicon carbide-on-insulator (4H-SiCOI) serves as a novel and high efficient integration platform for nonlinear optics and quantum photonics. The realization of wafer-scale fabrication of single-crystalline semi-insulating 4H-SiC film on Si (100) substrate using the ion-cutting and layer transferring technique was demonstrated in this work. The thermodynamics of 4H-SiC surface blistering is investigated via observing the blistering phenomenon with a series of implanted fluences and annealing temperatures. Surface tomography and the depth dependent film quality of the 4H-SiC have been extensively studied by employing scanning electron microscopy (SEM) and transmission electron microscopy (TEM). Moreover, X-ray diffraction (XRD) was carried out and the diffraction spectrum reveals a narrow peak with a full width at half maximum (FWHM) of 75.6 arcsec, indicating a good maintenance of the single-crystalline phase for the prepared thin film of 4H-SiC as compared to its bulk counterpart. With the single-crystalline 4H-SiCOI, we have successfully fabricated a micro-ring resonator with a quality factor as high as 6.6×10^4. The reported 4H-SiCOI wafer provides a feasible monolithic platform for integrated photonic applications.

Keywords: 4H-silicon carbide-on-insulator platform, wafer-scale, ion-cutting and layer transferring, surface blistering, nonlinear optical device

1. Introduction

In recent years, more and more researches focus on silicon carbide (SiC) because of its unique material properties including large band gap (2.4 – 3.2 eV), high physical hardness, high thermal conductivity (480 W m^{-1} K^{-1}), chemical inertness, large quadratic (χ^2) nonlinearity (30 pm V^{-1}) and Kerr nonlinearity (10^{-18} m^2 W^{-1}). The great interest is that SiC hosts a variety of promising color centers which could be able to be engineered as all-solid-state single-photon sources with broad spectral emission range [1-3]. Given its unique material and optical properties, SiC has emerged as one of the most promising materials for nonlinear optical devices and quantum photonic applications. So far more than 200 polytypes of crystalline structures for SiC have been reported, and among them three of the polytypes dominate. They are 3C (cubic, T_d^2 space group), 4H (hexagonal C_{6v}^4, space group) and 6H (hexagonal C_{6v}^4, space group) with band gaps of 2.4, 3.2, and 3.0 eV respectively [4-6]. It is worth noticing that 4H-SiC is the most promising polytype material arising from its large band gap which determines a large transparency window (0.37 – 5.6 μm) in optical applications[7]. Servicing as a nonlinear optical platform, a SiC layer on silicon (100) substrate with a low-refractive-index oxide layer in between, *i.e.*, SiC-SiO_2-Si, is required. However, previous devices were limited to polycrystalline 3C-SiC film which was epitaxially grown on silicon substrate without the intermediate oxidize layer, which renders the integrated photonic circuits inconvenient. In addition, there are lots of stacking defects in the hetero-epitaxially grown 3C-SiC thin film due to the lattice mismatch between 3C-SiC and silicon, which has proven to be detrimental for the high-performance optical devices [7-11]. In addition, devices based on amorphous SiC with SiO_2 layer was also reported in recent years[12]. However, amorphous SiC shows compromised mechanical and nonlinear optical properties compared to the crystalline SiC. In the other hand, the SiC bulk thinning technique shows better property due to recent work, but the large deviation of the SiC film thickness limited the scale of the devices[13]. The high-quality crystalline SiC thin film based on silicon substrate in wafer-scale still needs further development.

In this work, the full 4-inch wafer-scale semi-insulating 4H-SiCOI substrate is reported. The SiCOI wafers are fabricated by ion-cutting and layer transferring technique which has been

applied in mass production of silicon-on-insulator (SOI) wafers. Such technique shows the possibility to transfer single-crystalline 4H-SiC film on Si (100) substrate [14-18]. The 4H-SiC film are transferred to SiO_2/Si substrate from the bulk 4H-SiC wafer, so the density of dislocation and crack depends on the quality of the bulk 4H-SiC. Moreover, the quality of 4H-SiC thin film will not be affected by the lattice mismatch between SiC wafer and the substrate, so the high-quality single-crystalline 4H-SiC film directly transferred to SiO_2/Si (100) substrate could be achieved. The thermodynamics of 4H-SiC surface blistering is investigated via observing the blistering phenomenon with a group of implantation fluences and annealing temperatures. By using the 4H-SiC film on SiO_2/Si substrate, we have demonstrated a micro-ring resonator working at telecom wavelength and its intrinsic quality factor is up to 6.6×10^4. The presented work introduces a 4H-SiCOI material platform for integrated photonic applications.

2. Experimental methods

The fabrication process of heterogeneous SiC on Si (100) substrate using the typical ion-cutting and layer transferring technique is schematically shown in Fig. 1(a)-(d), which combines ion-cutting and wafer bonding. First of all, a 4-inch 4H-SiC wafer was implanted by 115 keV H^+ ions with fluences from 1×10^{16} to 9×10^{16} cm^{-2} at room temperature (RT) with a beam flux of 3×10^{12} cm^{-2} s^{-1} as shown in Fig. 1(a). It should be noted that the 4H-SiC wafer was tilted by 7° in order to minimize the ion channel effect during the implantation process. Then a damaged layer below the implantation surface was induced by the H^+ implantation and the depth can be controlled by changing the implantation energy. After the H^+ implantation, the 4H-SiC wafer and a thermally oxidized Si (100) substrate were treated by the standard chemical cleaning procedure with RCA solution. Thereafter the surfaces of the two wafers were treated by oxygen (O_2) plasma for 30 seconds in order to make the surfaces hydrophilic. Next, the SiC wafer and Si substrate were directly bonded at room temperature as shown in Fig. 1(b). After annealing at 810 °C in N_2 atmosphere for 1 hours, the 4H-SiC thin film blistered from the 4H-SiC wafer and subsequently transferred to the SiO_2/Si substrate as shown in Fig. 1(c). In order to enhance the bonding strength and to recover the ion implantation induced damage [18, 19], the 4H-SiCOI wafer was further post-annealed at 1100 °C for 10 hours. After further chemical mechanical polishing (CMP) process, a micro-ring resonator structure was patterned by using electron beam lithography (EBL). The final structure was transferred to 4H-SiCOI wafer by employing an inductively coupled plasma

reactive ion etching (ICP-RIE) with fluorine-based gases (SF_6) and O_2 [20, 21]. Next, the waveguide was annealed in oxygen atmosphere at 1100 °C and treated by 5% HF in order to suppress the roughness of the sidewall of the micro-ring resonator. At the end, the whole structures is cladded with a layer of SiO_2 by using Low-Pressure Chemical Vapor Deposition (LPCVD) followed by Plasma-Enhanced Chemical Vapor Deposition (PECVD) [7].

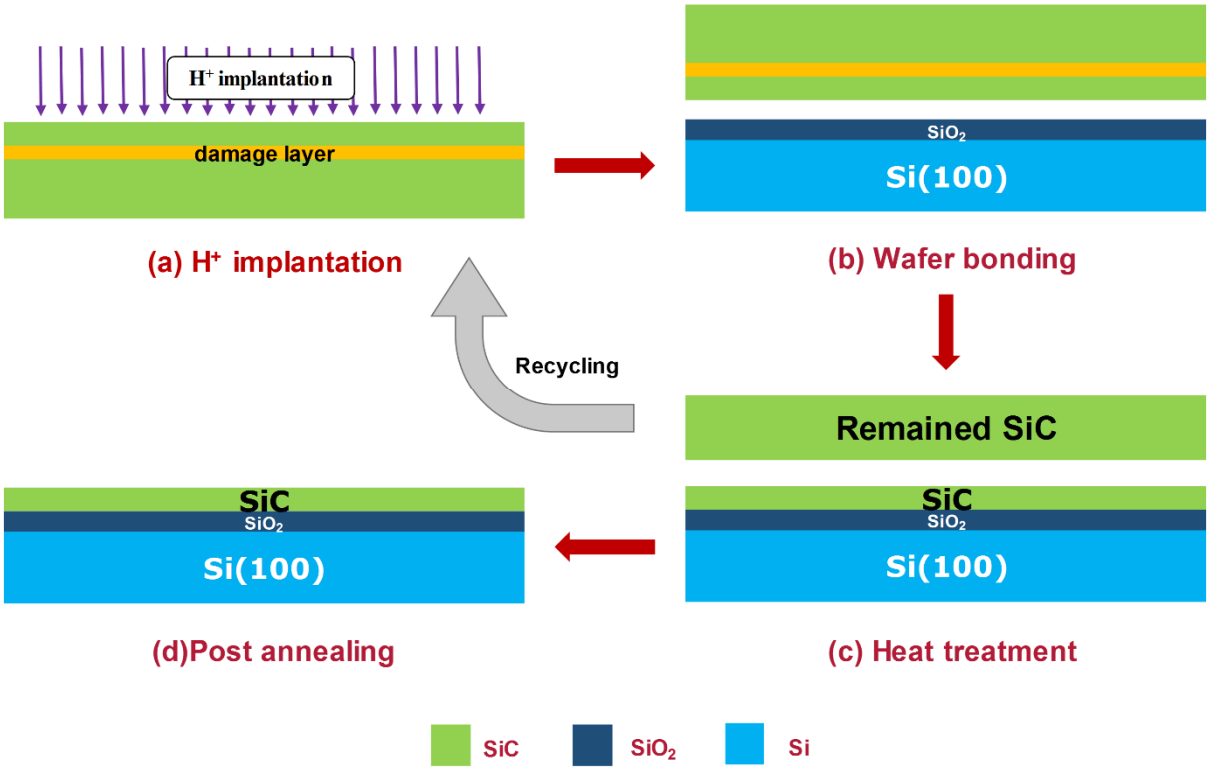

Figure 1. Heterogeneous integration of SiC film with Si(100) substrate using the ion-cutting method. (a) Implanting H^+ ions into the SiC wafer; (b) Cleaning and bonding SiC with Si(100) handle wafer; (c) Annealing and transferring the SiC film onto the Si(100) substrate; (d) Post-annealing to enhance the bonding strength and to recover the damage and defect due to the implantation.

The single-crystalline quality of the 4H-SiC film was characterized by X-ray diffraction (XRD) rocking curves along the (0004) plane using the Philips X'Pert X-ray diffractometer. The surface topography of the 4H-SiC film was characterized by the Bruker Multimode 8 atomic force microscopy (AFM) at tapping mode before and after CMP process. The defects and lattice dislocations in the SiC/SiO_2 cross section were characterized using scanning electron microscope (SEM), cross-sectional transmission electron microscopy (XTEM), high resolution transmission electron microscopy (HRTEM), selected area electron diffraction (SAED) and scanning transmission electron microscopy (STEM) using JEM-ARM300F Cs-corrected Transmission Electron Microscope. In addition, optical spectrum analyzer (OSA),

external-cavity lasers (ECLs), polarization controllers (PCs) and lensed fiber were used for the measurement of the micro-ring resonator.

3. Thoery

As mentioned above, the RCA treated bonding surfaces are hydrophilic and mainly terminated by OH groups. The mechanism of (0001) surface of SiC wafer and oxide covered Si (100) wafer bonding is just similar to the conventional Si-Si bonding. We know that the polymerization of silanol groups (Si-OH) can take place at room temperature and form strong siloxane (Si-O-Si) covalent bonds if the groups are in proximity. The reaction at bonding surface could be express as:

$$\text{Si-OH} + \text{OH-Si} \leftrightarrow \text{Si-O-Si} + H_2O. \quad (1)$$

Post-annealing is necessary because reaction (1) is reversible at T < 425 °C if water molecules are present. The excess water molecules have to be removed in order to form strong siloxane bonds (Si-O-Si) across the bonding surfaces[17]. Water molecules could be removed that bridge across the bonding wafer via annealing at T > 110 °C. Some water molecules could slowly diffuse along the bonding interface to the outside, and some could also diffuse through the surrounding thermal or native oxide to react with silicon and form SiO_2 and hydrogen:

$$Si+2H_2O \rightarrow SiO_2+2H_2. \quad (2)$$

In addition, the influence to the bonding strength of carbon element is limited because the natural oxidational layer on the (0001) surface.

It is critical to understand the basic mechanism of the crack formation in H^+-implanted 4H-SiC in order to optimize the ion-cutting process. Actually, many investigations have been reported on the ion implantation and exfoliation of SiC[22, 23]. In present work, the topography variation on the surface of 4H-SiC implanted with different H^+ fluences and annealing temperatures was recorded in optical micrographs, as shown in Fig. 2. As far as conclusions are concerned, a well defined temperature exists at which blisters start appearing. For the lower implantation fluence with 5×10^{16} cm^{-2} H^+ samples as shown in Fig. 2(a), (b) and (c), no blisters appeared on the surface even annealed at 900 °C for 6 hours. For the sample

implanted by H^+ at the fluence of 6×10^{16} cm^{-2}, the surface blistered and exfoliated after annealing at 800 °C for 6 hours. In addition, no blisters appeared in the sample after annealing at 790 °C for 6 hours as shown in Fig. 2(d). Therefore, the threshold temperature for blistering of SiC lattice should be close to 800 °C. As shown in Fig. 2(f), the blister process finished in 1 hour at 810 °C which is beyond the threshold temperature. In addition, the samples implanted by the highest H^+ fluence of 7×10^{16} cm^{-2} have a lower threshold temperature as shown in Fig. 2(g), (h) and (i). No blistering phenomenon was observed until increasing annealing temperature to 780 °C. Fig. 2(f) and (h) illustrate two types of blister evolution during annealing. Some blisters grew up continuously and finally cracked as shown in Fig. 2(f). Some blisters grew up at the beginning but shrank with the annealing time increasing as shown in Fig. 2(h) in the contrast.

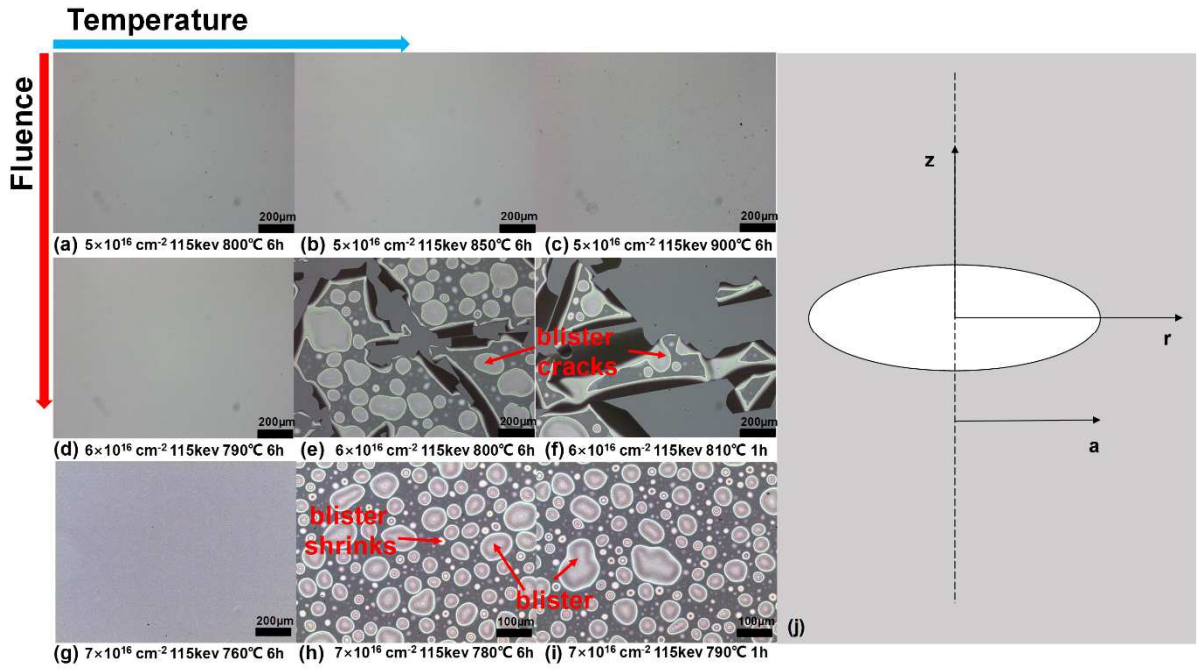

Figure.2 (a)-(i) A series of 4H-SiC samples implanted with different H^+ fluences at 115 keV and annealed with various recipe in argon ambient as indicated. Optical micrographs show blisters and exfoliated flakes. Different figures represent independent samples and are numbered in the order in which they were annealed (there are no multiple anneals of the same sample). (j) The schematic diagram of the thermodynamic model.

The thermodynamics of H^+-implanted SiC was analyzed based on the model for Si proposed by Han et al [24]. This model was investigated by blistering experiments of Si and Ge and it was also verified by GaN blistering research[25]. Fig. 2(j) shows the schematic diagram of a planer crack with the radius a determined by the crack energy Γ, the strain energy U of bulk SiC around blister, and the external potential energy W. The total free energy of a growing

hydrogen blister is

$$G(a,T) = W(a) + U(a) + \Gamma(a,T) \quad ,$$

(3)

The criterion for blister growth is taken to be $\frac{\partial G(a,T)}{\partial a} = 0$ according to the Griffith energy condition. The critical radius for crack is given as

$$a_{crit} = \frac{\pi\gamma(T)E}{0.18p^2(1-\nu^2)} \quad ,$$

(4)

where γ(T) is the surface tension as a function of annealing temperature T, E is Young's modules, p is the hydrogen pressure, and υ is Poisson ratio. The blister is not thermally stable and it will grow up and then crack while a > a_{crit}. In the other hand, the blister will shrink in the case of a<a_{crit}. The crack and shrink phenomenon are marked with red arrow as shown in Fig. 2(e) and (g), respectively. When G(a)=0, the blister growth will stop and the maximum radius should be a_{max}=1.5a_{crit}[24]. H^+ implantation mainly causes lattices dislocation and displacement of the Si and C atoms. Point defects formed by the collision cascades of these displaced Si and C atoms. Implanted H^+ reacts with a part of the defects to form complexes VH_n, V_nH and Si, C atoms to form chemical bonds Si-H, C-H[26, 27]. The trapped H dislocated from the complexes and bonds with a binding energy E_a and assembled with a diffusion energy E_d. The blisters grew up while the initial pressure induced stress exceeded the fracture toughness of SiC, also accompanied by the pressure decreasing. It is assumed that the H^+ implantation fluence is ϕ_0 and the releasing H^+ fluence during annealing is ϕ_e. Then the H_2 generation rate from the implanted region could be express as

$$\frac{\partial \phi_e(t,T)}{\partial t} = -k\phi_e(t,T) \quad ,$$

(5)

and the reaction rate constant is

$$k = \frac{1}{\tau}\exp\left(-\frac{E_a + E_d}{k_B T}\right) \quad ,$$

(6)

where T is the annealing temperature, τ is the phenomenological parameter which is related to the stretching frequency of the dissociating complexes and Si-H, C-H bonds. k_B is the

Boltzmann's constant [28]. The activation energy of SiC crack $E_A = E_a+E_d$ is about 3.0 eV according to previous research [29].

If the annealing time t is long enough, all the H^+ ions shall be released which is equally to ϕ_0

$$\phi_0 = \int_0^\infty \phi_e(t,T)dt \quad .$$

(7)

Combine with Eq. (5), (6) and (7), we could know

$$\phi_e(t,T) = k\phi_0 \exp(-kt). \quad (8)$$

The number of H_2 molecules which contributed to the generation of SiC surface crack is

$$N = \pi a^2 \int_0^t \phi_e(t,T)dt = \frac{\pi a^2 k\phi_0}{\exp\left(\frac{1}{kt}\right)} \quad .$$

(9)

Eq. (9) shows that more H_2 molecules diffuse into the micro-crack to pressurize the volume and cause the surface blistering with the annealing time increasing.

In addition, the blister radius could be described as a function

$$a(t,T,\phi_0) = \frac{3\pi E\phi_0[1-\exp(-kt)]k_BT}{16(1-\nu^2)p^2}. \quad (10)$$

In the formula, p is determined by the fracture toughness of SiC and the blister radius. Just as the ion-cutting of Si[24], the fluence window also exists for SiC. Indeed, there is an optimized fluence for the ion-cutting process of SiC. The extent of the exfoliation increases with increasing fluence below the optimized fluence while it decreases with increasing fluence above the optimized fluence. The thermodynamic model is only suitable for the case of H^+ fluence below the optimized fluence because the negative effect of ultra-high H^+ fluence is not concerned. In this work, the model is still worked as the blister was not observed until the fluence increased to 6×10^{16} cm^{-2}[14, 19].

The annealing time t could be defined as $t = \infty$ when t is long enough, as the a will be $a(\infty, T, \phi_0) = a_{max} = 1.5a_{crit}$. For the case of $\phi_0 = 6\times10^{16}$ cm^{-2}, with Eq. (4) and (10), the crack surface

tension of the blister γ(T) could be calculated as $\gamma(T) = 1.863\times10^{-4}$ T J m^{-2}.

When the SiC surface begins to split, the radius of the blister should be equal to the critical radius a_{crit}. Combining Eq. (6) and (9), we could express the crack time as a function of annealing temperature as

$$t(T) = -\tau \exp\left(\frac{E_a + E_d}{k_B T}\right)\ln\left(1-\frac{29.6\gamma(T)}{k_B T \phi_0}\right). \quad (11)$$

In comparison with Si, SiC has a much higher activation energy (3.0 eV to 1.8 eV) [30]. Thus, with the same annealing time t, the trapped H is much difficult to be released to generate H_2 in SiC which causes the much higher blistering temperature of SiC compared to the same case of Si (810 °C to 450 °C)[31]. In addition, L. B. Freunde reported an ideal formula which shows the minimum fluence for surface blistering given as $\phi_{\min} = \frac{8}{3}\frac{\gamma}{k_B T}$ [32]. According to previous calculation, the minimum fluence for 4H-SiC blistering could be estimated to be 3.6×10^{15} cm^{-2}. However, the blistering phenomenon was not observed until we increased the H^+ fluence to 6×10^{16} cm^{-2}. Only 6% of the total implanted H^+ ions are effective for the SiC surface blistering. During annealing process, most of the implanted H^+ were still be trapped by chemical bonds with Si and C atoms and only a small part of the implanted H^+ was released for the formation of H_2 which caused the surface blistering according to the calculation result.

4. Results and Discussions

4.1. Thickness Deviation

The 4H-SiC thin film were successfully transferred to Si (100) substrate as shown in Fig. 3(a). Over 95% of the SiC thin film was successfully transferred onto the Si (100) wafer. Fig. 3(b) shows the thickness mapping measured from 41 uniformly distributed points of the as-transferred SiC film by white light interferometer. The average thickness of the as-transferred SiC thin film is 1102.2 nm and the thickness deviation is +/- 0.2% calculated by the following formula.

$$deviation = \frac{(T_{Max} - T_{Min})}{2\times T_{Mean}}\times 100$$

where T_{Max}, T_{Min} and T_{Mean} are the maximum thickness, minimum thickness and average

thickness, respectively.

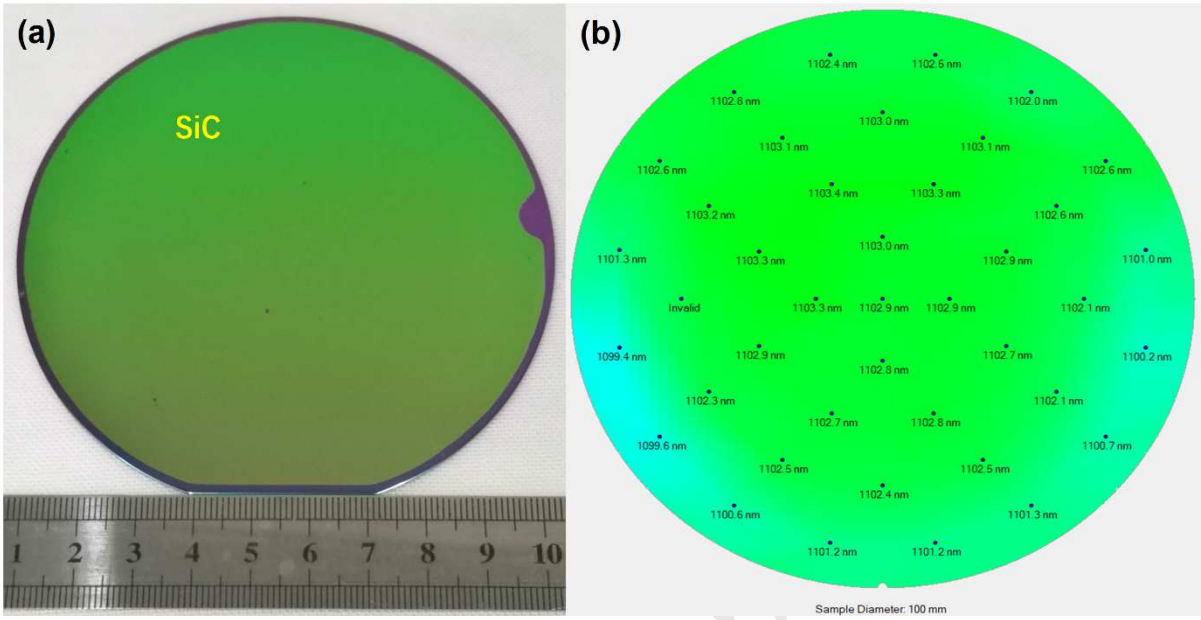

Figure 3 (a) Photograph of 4-inch wafer-scale 4H-SiCOI substrate fabricated using ion-cutting and layer transferring technique. (b) The thickness homogeneity of SiC film was measured by white light interferometer.

4.2. XRD Measurement

The OM image of the 4H-SiC film surface is shown in the inset of Fig. 4(a) as the scale is 100 μm. No crack was observed on the 4H-SiC film. The crystalline quality of the SiC film was evaluated by X-ray rocking curves (XRCs) measurements. Usually, the values of strain in the near surface region and in the highly damage region are given by the position of the satellite peak and the Bragg peak, respectively. The position of the peak at the lower angle side decides the H^+-implantation-induced elastic strain. Due to the peak located at the lower angles, a dilation of lattice parameter along the direction perpendicular to the specimen surface is regarded. For peak at the higher angles, the case is opposite. The normalized symmetric (0004) XRC for the virgin 4H-SiC, the as transferred 4H-SiC film and the 4H-SiC post-annealed at 1100 °C are shown in Fig. 4(a). The full width at half maximum (FWHM) of the (0004) XRC for the virgin 4H-SiC is 25.8 arcsec, while the FWHM of the as-transferred 4H-SiC film is 288 arcsec. A satellite peak at higher angle of the main Bragg peak was observed in the as-transferred 4H-SiC thin film, which indicates that the H^+ implantation induced thin film exfoliation introduces significant out-of-plane compressive strain. The compressive strain is mainly caused by two factors. The one is induced by the increase of the pressure and volume of the blisters during the exfoliation process. The other is due to the

thermal stress caused by the difference of thermal expansion coefficient between SiC ($4.5\times10^{-6}\,K^{-1}$) and Si ($2.5\times10^{-6}\,K^{-1}$). Si was compressed by SiC wafer during the heat treatment which caused the tensile strain along the SiC (0001) plane corresponding to the compressive strain out-of-(0001) plane along <0001> orientation. The thermal stain was remained even the SiCOI wafer cooled down due to the plastic deformation of Si under 800 °C annealing. The satellite peak shifts from the main Bragg peak by $\Delta\omega$=212.4 arcsec at the right side, corresponding to a 0.32% out-of-plane compressive strain in the as-transferred film. After annealing at 1100 °C for 10 hours, the crystalline quality of the SiC thin film was recovered, and the FWHM was decreased to 75.6 arcsec as indicated by the blue curve in Fig. 4(a). The strain was completely released as there is no significant satellite peak observed in the blue curve in Fig. 4(a).

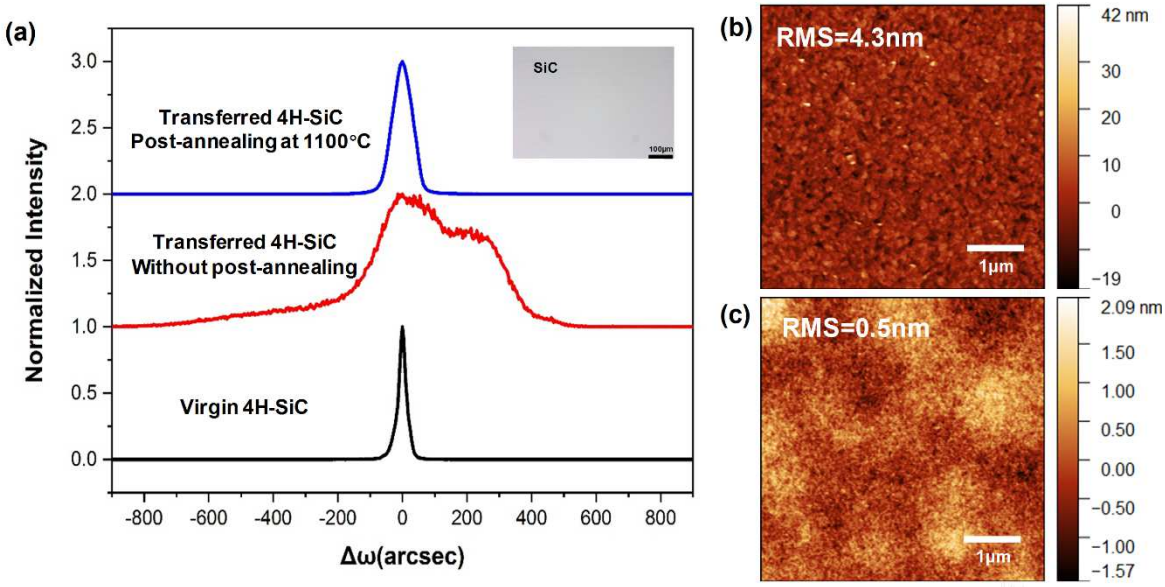

Figure.4 (a) The (0004) XRC for the virgin 4H-SiC, as-transferred 4H-SiC film and SiC film post-annealed at 1100 °C. (b) AFM images of as-transferred 4H-SiC film, and RMS roughness is 4.3 nm. (c) AFM images of 4H-SiC film after ion milling, and RMS roughness is 0.5 nm.

4.3. AFM Measurement

The surface roughness of 4H-SiC film was evaluated by Atom Force microscopy (AFM) as shown in Fig. 4(b) and (c). The surface of the as-transferred SiC film is quite rough with a roughness (RMS) of 4.3 nm in a scanning area of 5 μm×5 μm. After 1100 °C post-annealing, in order to achieve a smooth SiC film surface, the SiC surface was then optimized by CMP treatment as shown in Fig. 4(c). After CMP treatment, the RMS is reduced from 4.3 nm to 0.5

nm.

4.4. TEM Measurement

Fig. 5(a) shows the SEM image of the as-prepared 4H-SiCOI substrate after annealing process and CMP. The sharp interfaces of SiC/SiO_2 and SiO_2/Si were observed. Fig. 5(b) shows the XTEM images of the $(11\bar{2}0)$ face of optimized 4H-SiC film. The thickness of the SiC film is about 747 nm. Fig. 5(c)-(f) show the HRTEM images in different regions from top to bottom of the SiC thin film. The amorphous region is about 11nm among the SiC film surface in Fig. 5(c). This part is mainly consisted of Si and O according to the EDS measurement. The surface of the polished SiC is easily to be oxidized because of the oxidant composition in the slurry for CMP. From the HRTEM images in Fig. 5(c)-(f), the periodic lattice fringe can be clearly observed from the top, middle, and bottom region of the SiC thin film, which suggests the SiC thin film are of high single-crystalline quality. The single-crystalline quality could also be confirmed by the selected area electrons diffraction (SAED) shown in the insets in Fig. 5(e)-(f), which illustrate the regular single-crystal diffraction patterns. The poly region about 2 nm among the bonding interface is because of the reaction of Si-OH and the diffusion effect between SiC and SiO_2 during annealing process. In addition, as the 4H crystal formation, the periodic arrangement of Si and C atoms for four layers circle could be clearly observed through the inset STEM images. After removing the top amorphous layer by hydrofluoric acid (HF) treatment, a high-quality single-crystalline SiC thin film was obtained.

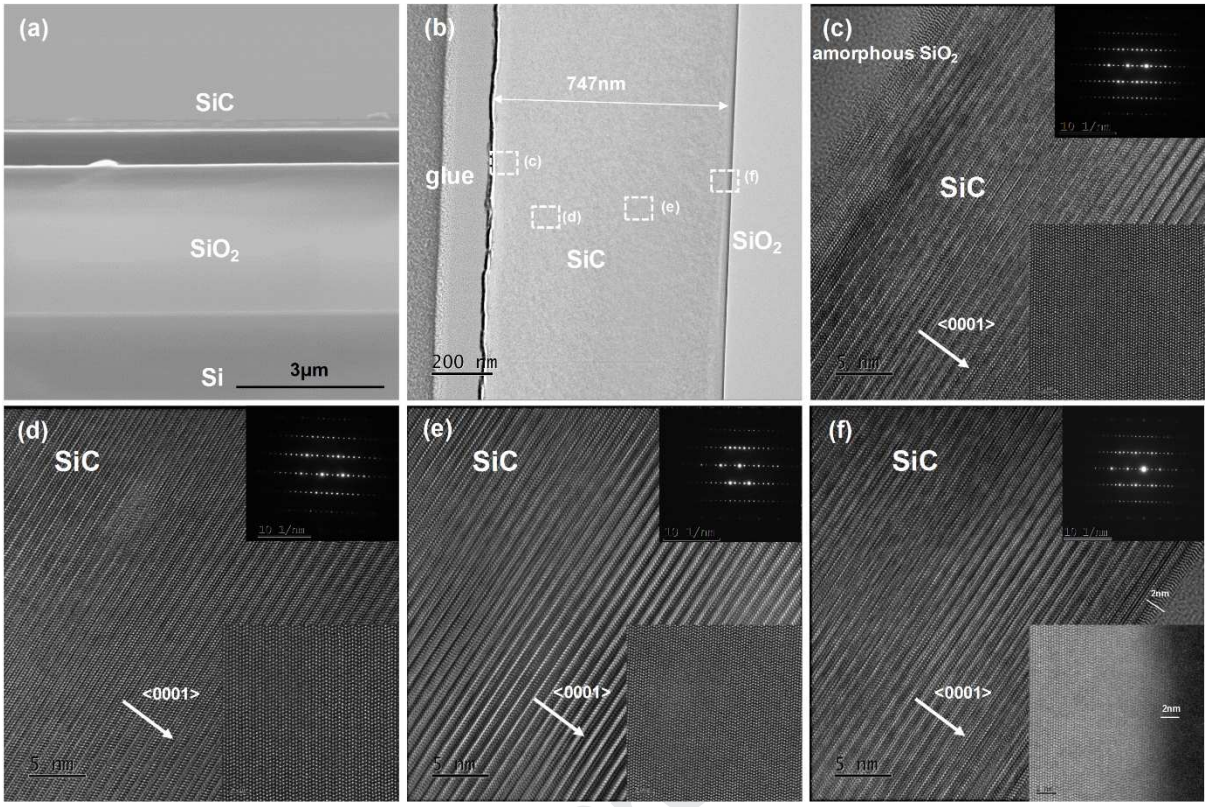

Figure.5 (a) Cross sectional SEM image of the optimized 4H-SiCOI (post-annealed at 1100 °C after CMP). (b) XTEM image of the optimized 4H-SiCOI. (c)-(f) HRTEM, STEM images and SAED patterns taken from the area marked in (b).

4.5. Micro-Ring Resonator

In order to demonstrate the SiCOI as a feasible monolithic platform for integrated photonic applications, optical resonators were fabricated on the SiCOI substrate by a standard lithography process. The SEM images in Fig. 6(a), (b), (c) show a micro-ring resonator with a radius of 16.5 μm. Fig. 7(a) shows the normalized transmission spectra the micro-ring resonators for transverse electric (TE) mode, and the inset in Fig. 7(a) is simulated mode profiles with an effective mode area of 0.26 μm^2 for fundamental TE mode. Fig. 7(b) is the resonances fitting of micro-ring resonators for fundamental TE modes for wet etched samples, where the measured intrinsic Qs is up to 66000 and coupling loss is 3.5 dB $facet^{-1}$ based on spot size of 3.5 μm.

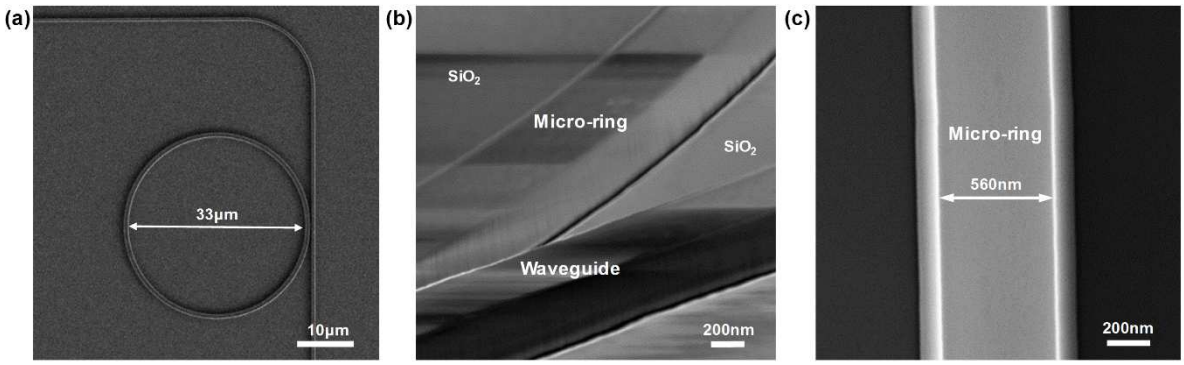

Figure.6 (a) Top-view SEM image of fabricated micro-ring resonator with radius of 16.5 μm based on SiCOI platform. (b) Zoom in SEM image of the bus-to-ring region and the side wall of the micro-ring and waveguide. (c) The top-view of high resolution SEM image of the micro-ring with the width of 560 nm.

Fig. 7(d) shows the Qs of TM mode could be up to 48000. H^+ implantation and exfoliation process mainly generated platelets cracks, lattices disorder and vacancy clusters in the SiC film [33, 34]. The TEM illustration reveals that the all the dislocation were recombined except for the vacancy clusters after post-annealing at 1100 °C and CMP treatment according to Fig. 5. The remained vacancies is the main reason for the light loss. To further optimize the performance of devices, the quality of SiC thin film could be improved by H^+ implantation at elevated temperature and by post-annealing at an even higher temperature in order to minimize the implant-induced defects.

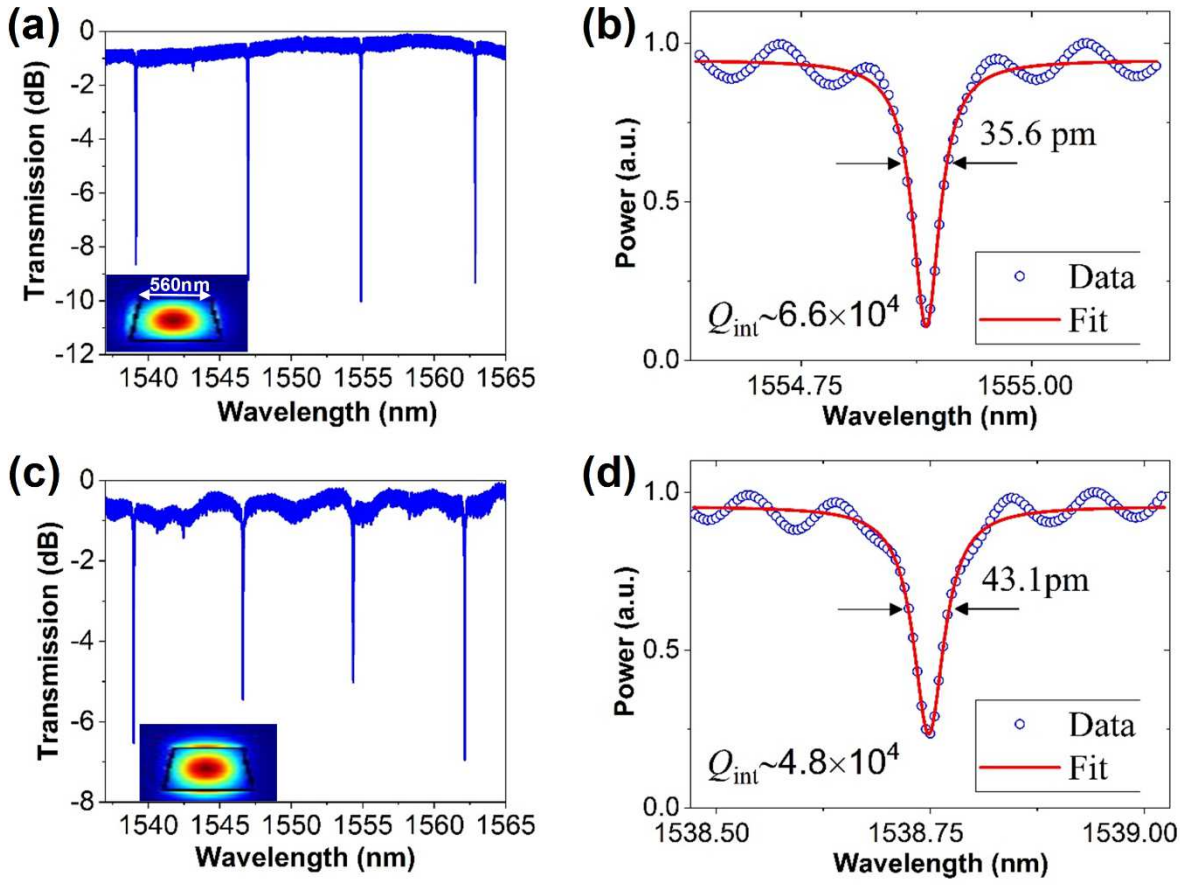

Figure.7 (a), (c) Measured (normalized) transmission spectra for a 16.5-μm radius micro-ring resonator for fundamental TE mode and TM mode, respectively. (b), (d) Resonance fittings for fundamental TE modes and TM modes of micro-ring resonators, respectively.

5. Conclusion

In conclusion, 4-inch single-crystalline 4H-SiC film have been successfully integrated with Si (100) substrate coated with 2μm thermal SiO_2 layer by using the ion-cutting and layer transferring technique. Over 95% of the SiC thin film was transferred onto the Si wafer. After post-annealing at 1100 °C, the FWHM of SiC film is 75.6 arcsec. The single-crystalline quality of SiC film was demonstrated by SEM and XTEM measurement. In addition, optical resonator devices based on SiCOI platform were demonstrated. The intrinsic Qs of resonances fitting of micro-ring resonators for fundamental TE modes and TM modes were measured to be 66000 and 48000, respectively. The property of the resonator can be further improved by removing the implantation damage remained in the SiC film. This can be achieved by employing the H^+ implantation at elevated temperatures and by post-annealing at a higher temperature.

Acknowledgement

This work was supported by National Natural Science Foundation of China (No. U1732268, 61874128, 11622545, 61851406, 11705262 and11905282), Frontier Science Key Program of CAS (No. QYZDY-SSW-JSC032), Chinese−Austrian Cooperative R&D Project (No. GJHZ201950), Shanghai Science and Technology Innovation Action Plan Program (No. 17511106202), Program of Shanghai Academic Research Leader (19XD1404600), Shanghai Sailing Program (No. 19YF1456200, 19YF1456400), K.C.Wong Education Foundation (GJTD-2019-11) and Danish National Research Foundation (DNRF123).

Reference

[1] J. Cardenas, M. Yu, Y. Okawachi, C.B. Poitras, R.K. Lau, A. Dutt, A.L. Gaeta, M. Lipson, Opt Lett, 40 (2015), pp. 4138-4141.
[2] S. Castelletto, B.C. Johnson, V. Ivády, N. Stavrias, T. Umeda, A. Gali, T. Ohshima, Nature Materials, 13 (2013), p. 151.
[3] H.-P. Phan, D.V. Dao, K. Nakamura, S. Dimitrijev, N.-T. Nguyen, Journal of Microelectromechanical Systems, 24 (2015), pp. 1663-1677.
[4] M. Radulaski, T.M. Babinec, S. Buckley, A. Rundquist, J. Provine, K. Alassaad, G. Ferro, J. Vuckovic, Opt Express, 21 (2013), pp. 32623-32629.
[5] P.G. Baranov, A.P. Bundakova, A.A. Soltamova, S.B. Orlinskii, I.V. Borovykh, R. Zondervan, R. Verberk, J. Schmidt, Physical Review B, 83 (2011), p.125203.
[6] G. Calusine, A. Politi, D.D. Awschalom, Applied Physics Letters, 105 (2014), p. 011123.
[7] Y. Zheng, M. Pu, A. Yi, B. Chang, T. You, K. Huang, A.N. Kamel, M.R. Henriksen, A.A. Jorgensen, X. Ou, H. Ou, Opt Express, 27 (2019), pp. 13053-13060.
[8] T. Fan, H. Moradinejad, X. Wu, A.A. Eftekhar, A. Adibi, Opt Express, 26 (2018), pp. 25814-25826.
[9] F. Martini, A. Politi, Applied Physics Letters, 112 (2018), p. 251110.

[10] X. Lu, J.Y. Lee, P.X. Feng, Q. Lin, Opt Lett, 38 (2013), pp. 1304-1306.
[11] X. Lu, J.Y. Lee, S. Rogers, Q. Lin, Opt Express, 22 (2014), pp. 30826-30832.
[12] P. Xing, D. Ma, K.J.A. Ooi, J.W. Choi, A.M. Agarwal, D. Tan, ACS Photonics, 6 (2019), pp. 1162-1167.
[13] D.M. Lukin, C. Dory, M.A. Guidry, K.Y. Yang, S.D. Mishra, R. Trivedi, M. Radulaski, S. Sun, D. Vercruysse, G.H. Ahn, J. Vučković, Nature Photonics, (2019).
[14] B. Terreault, physica status solidi (a), 204 (2007), pp. 2129-2184.
[15] B.S. Li, Z.G. Wang, J.F. Jin, Nuclear Instruments and Methods in Physics Research Section B: Beam Interactions with Materials and Atoms, 316 (2013), pp. 239-244.
[16] K. Mitani, U.M. Gösele, Journal of Electronic Materials, 21 (1992), pp. 669-676.
[17] T. Höchbauer, A. Misra, M. Nastasi, J.W. Mayer, Journal of Applied Physics, 92 (2002), pp. 2335-2342.
[18] B. Wang, B. Gu, H. Zhang, X. Feng, Acta Mechanica Solida Sinica, 29 (2016), pp. 111-119.
[19] R.B. Gregory, T.A. Wetteroth, S.R. Wilson, O.W. Holland, D.K. Thomas, Applied Physics Letters, 75 (1999), pp. 2623-2625.
[20] R. Yang, K. Ladhane, Z. Wang, J. Lee, D.J. Young, P.X.L. Feng, Smart-cut 6H-silicon carbide (SiC) microdisk torsional resonators with sensitive photon radiation detection, Proceedings of the IEEE International Conference on Micro Electro Mechanical Systems (MEMS)2014, pp. 793-796.
[21] H. Jia, J.S. Lee, Z.H. Wang, P.X.L. Feng, 2014 Ieee International Frequency Control Symposium (Fcs), (2014), pp. 24-27.
[22] Q. Jia, K. Huang, T. You, A. Yi, J. Lin, S. Zhang, M. Zhou, B. Zhang, B. Zhang, W. Yu, X. Ou, X. Wang, Applied Physics Letters, 112 (2018), p. 192102.
[23] N. Daghbouj, B.S. Li, M. Karlik, A. Declemy, Applied Surface Science, 466 (2019), pp. 141-150.
[24] W. Han, J. Yu, Journal of Applied Physics, 89 (2001), pp. 6551-6553.
[25] Q.Y. Tong, K. Gutjahr, S. Hopfe, U. Gösele, T.H. Lee, Applied Physics Letters, 70 (1997), pp. 1390-1392.
[26] S.W. Bedell, W.A. Lanford, Journal of Applied Physics, 90 (2001), pp. 1138-1146.
[27] M. Ionescu, A. Deslandes, R. Holmes, M.C. Guenette, I. Karatchevtseva, G.R. Lumpkin, Materials Science Forum, 879 (2016), pp. 810-814.
[28] V.P. Amarasinghe, L. Wielunski, A. Barcz, L.C. Feldman, G.K. Celler, ECS Transactions, 50 (2013), pp. 341-348.
[29] V.P. Amarasinghe, L. Wielunski, A. Barcz, L.C. Feldman, G.K. Celler, Ecs Journal of Solid State Science and Technology, 3 (2014), pp. P37-P42.
[30] Q. Tong, T. Lee, L. Huang, Y. Chao, U. Gosele, Electronics Letters, 34 (1998), pp. 407-408.
[31] J. Neugebauer, C.G. Van de Walle, Phys Rev Lett, 75 (1995), pp. 4452-4455.
[32] L.B. Freund, Applied Physics Letters, 70 (1997), pp. 3519-3521.
[33] Y. Wang, Y. Liu, E. Wendler, R. Hübner, W. Anwand, G. Wang, X. Chen, W. Tong, Z. Yang, F. Munnik, G. Bukalis, X. Chen, S. Gemming, M. Helm, S. Zhou, Physical Review B, 92 (2015), p.174409.
[34] L. Zhang, B.S. Li, Physica B: Condensed Matter, 508 (2017), pp. 104-111.

Highlights

1. First demonstration of wafer-scale (4-inch) single-crystalline 4H-SiC film integrated with Si (100) substrate serves as a platform for nonlinear integrated optical devices.
2. The fabrication of the 4H-silicon carbide-on-insulator is demonstrated by ion-cutting and layer transferring technique. The thermodynamics of 4H-SiC surface blistering is theoretically analyzed and investigated via observing the blistering phenomenon with a series of implanted fluences and annealing temperatures.
3. In addition to the comprehensive material characterizations, micro-ring resonator devices with Q value of 6.6×10^4 based on 4H-SiCOI platform are demonstrated.

Author agreement

Dear Editor,

We the undersigned declare that this manuscript entitled “Wafer-scale 4H-silicon carbide-on-insulator (4H-SiCOI) platform for nonlinear integrated optical devices” is original, has not been published before and is not currently being considered for publication elsewhere.

We confirm that the manuscript has been read and approved by all named authors and that there are no other persons who satisfied the criteria for authorship but are not listed. We further confirm that the order of authors listed in the manuscript has been approved by all of us.

We understand that the Corresponding Author is the sole contact for the Editorial process. Prof. Xin Ou is responsible for communicating with the other authors about progress, submissions of revisions and final approval of proofs.

Signed by all authors as follows:

Dear editor, because of the 2019-conv virus in China, our organization is forced to stop work by the Chinese government. We guarantee that the manuscript has been approved by all the authors but it is difficult for us to contact all the authors for their signature during this time. We promise that the signature of all the authors will be added after we return to work.

Thank you very much!

Best Regards,
Xin Ou
Ailun Yi

Declaration of interests

☒ The authors declare that they have no known competing financial interests or personal relationships that could have appeared to influence the work reported in this paper.

☐The authors declare the following financial interests/personal relationships which may be considered as potential competing interests: